Inorganic Chemistry

Article

pubs.acs.org/IC

Asymmetrical Diruthenium Complex Bridged by a Redox-Active Ligand

Amit Das,[†] Thomas Michael Scherer,[‡] Abhishek Dutta Chowdhury,[†] Shaikh M. Mobin,[†] Wolfgang Kaim,*[,‡] and Goutam Kumar Lahiri*[,†]

[†]Department of Chemistry, Indian Institute of Technology Bombay, Powai, Mumbai 400076, India

[‡]Institut für Anorganische Chemie, Universität Stuttgart, Pfaffenwaldring 55, D-70550 Stuttgart, Germany

Supporting Information

ABSTRACT: The asymmetrical dinuclear complex $[(acac)_2Ru1(\mu\text{-abpy})Ru2(Cym)Cl]PF_6$ ($[\mathbf{2}]PF_6$), with $acac^-$ = acetylacetonato = 2,4-pentanedionato, abpy = 2,2′-azobis(pyridine), and Cym = *p*-cymene = 1-isopropyl-4-methylbenzene, has been obtained from the mononuclear precursors $[Ru(acac)_2(abpy)]$ and $[Ru(Cym)Cl_2]_2$. X-ray crystal structure analysis suggests the oxidation state formulation $[(acac)_2Ru1^{III}(\mu\text{-abpy}^{\bullet-})Ru2^{II}(Cym)Cl]^+$ for $\mathbf{2}^+$, with antiferromagnetic coupling between one Ru^{III} center and the radical-anion bridging ligand ($abpy^{\bullet-}$), based on the N−N distance of 1.352(3) Å. As appropriate references, the newly synthesized mononuclear $[(abpy)Ru^{II}(Cym)Cl]PF_6$ ($[\mathbf{1}]PF_6$) with an unreduced N═N double bond at d(NN) = 1.269(4) Å and the symmetrical dinuclear $[(acac)_2Ru^{2.5}(\mu\text{-abpy}^{\bullet-})Ru^{2.5}(acac)_2]$ with d(NN) = 1.372(4) Å (rac isomer) support the above assignment for $\mathbf{2}^+$ as an asymmetrical mixed-valent configuration bridged by a radical ligand. Reversible one-electron oxidation leads to a dication, $\mathbf{2}^{2+}$, with largely metal-centered spin (EPR: g_1 = 2.207, g_2 = 2.155, and g_3 = 1.929), and a weak intervalence charge-transfer absorption at 1700 nm, as observed by spectroelectrochemistry. These results support a description of $\mathbf{2}^{2+}$ as $[(acac)_2Ru1^{III}(\mu\text{-abpy}^0)Ru2^{II}(Cym)Cl]^{2+}$. Density functional theory (DFT) calculations suggest that the first reduction of $[\mathbf{2}]PF_6$ also involves the bridging ligand, leading to $[(acac)_2Ru1^{III}(\mu\text{-abpy}^{2-})Ru2^{II}(Cym)Cl]$ ($\mathbf{2}$). Experimentally, the first reduction of $\mathbf{2}^+$ is not fully reversible, with evidence for the loss of chloride to form $[(acac)_2Ru1(\mu\text{-abpy})Ru2(Cym)]^+$ ($\mathbf{2a}^+$; g_1 = 2.454, g_2 = 2.032, and g_3 = 1.947). Further reduction produces $[(acac)_2Ru1^{II}(\mu\text{-abpy}^{2-})Ru2^{II}(Cym)]$ ($\mathbf{2a}$), which forms $[(acac)_2Ru1^{II}(\mu\text{-abpy}^{2-})Ru2^{I}(Cym)]^-$/$[(acac)_2Ru^{II}(\mu\text{-abpy}^{\bullet-})Ru^0(Cym)]^-$ ($\mathbf{2a}^-$) in yet another one-electron step (g_1 = 2.052, g_2 = 2.008, and g_3 = 1.936). The major electronic transitions for each redox state have been assigned by time-dependent DFT calculations.

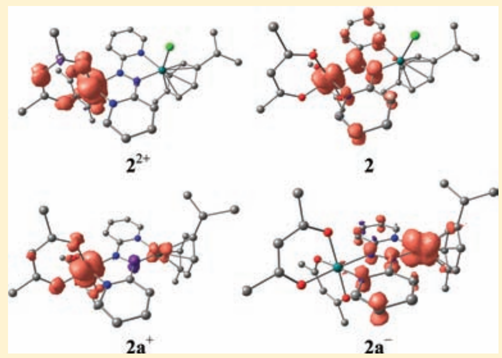

1. INTRODUCTION

The establishment of exact valence and spin distributions in polyruthenium frameworks incorporating redox-active ("noninnocent") bridging ligands is a formidable challenge, primarily because of the closeness of metal and ligand frontier orbitals.[1] The introduction of asymmetry in the framework can occur via the use of different metal ions, asymmetric bridges, or metal complex fragments with ancillary ligands of different electronic nature (π-accepting or σ/π-donating).[2] Besides the fundamental understanding of valence-exchange processes in the mixed-valent states of polyruthenium complexes,[1] there is a potential for the application of such materials in the design of molecular electronic[3] and optical information[4] devices.

In this context, the valence- and spin-exchange aspects of symmetrical diruthenium complexes with the noninnocent 2,2′-azobis(pyridine) (abpy) bridging ligand in compounds $[(acac)_2Ru(\mu\text{-abpy})Ru(acac)_2]^n$,[5] $[(bpy)_2Ru(\mu\text{-abpy})Ru(bpy)_2]^n$,[6] and $[Cl(Cym)Ru(\mu\text{-abpy})Ru(Cym)Cl]^n$[7] have been explored in recent years ($acac^-$ = acetylacetonato, bpy = 2,2′-bipyridine, and Cym = *p*-cymene). abpy is a well-known redox-active bridging ligand[8] that can exist as neutral abpy, as anion radical $abpy^{\bullet-}$, and as fully reduced $abpy^{2-}$, each with quite distinctive N−N bond distances (Scheme 1).

Scheme 1. Different Redox States of abpy with Corresponding N−N Bond Distances

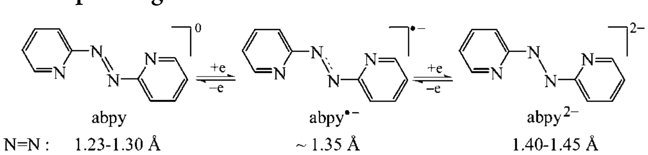

In order to understand the electronic situation in a nondegenerate polynuclear framework, an asymmetrical diruthenium complex, $[(acac)_2Ru1(\mu\text{-abpy})Ru2(Cym)Cl]^n$ ($\mathbf{2}^n$), has now been synthesized, where electronically different ruthenium fragments, $\{Ru(acac)_2\}$ encompassing σ-donating $acac^-$ and $\{Ru(Cym)Cl\}$ with π-accepting Cym, are bridged by the noninnocent abpy moiety.

$\{Ru(Cym)Cl\}$ has been chosen as one of the metal fragments in $[(acac)_2Ru1(\mu\text{-abpy})Ru2(Cym)Cl]PF_6$ ($[\mathbf{2}]PF_6$) because it is

Received: September 8, 2011
Published: January 17, 2012

expected to undergo Cl^- dissociation upon reduction with the concomitant formation of a low-valent coordinatively unsaturated metal site.[7,9] Such centers can function as effective substrate binding sites in homogeneous catalysis.[10]

Herein we report the synthesis and structural characterization of the reference mononuclear complex [Ru(abpy)(Cym)Cl]PF_6 ([**1**]PF_6) and of the asymmetrical dinuclear [(acac)$_2$Ru1-(μ-abpy)Ru2(Cym)Cl]PF_6 ([**2**]PF_6). The electronic situations in the accessible redox states of the complexes have been investigated by using electrochemistry, UV−vis−NIR spectroelectrochemistry, electron paramagnetic resonance (EPR) spectroscopy, and density functional theory (DFT) calculations. It should be noted that **2**$^+$ represents a rare example of a nondegenerate system in which the bridging ligand is redox-active.

2. RESULTS AND DISCUSSION

Synthesis and Characterization. The mononuclear complex [Ru^{II}(abpy)(Cym)Cl]PF_6 ([**1**]PF_6) has been prepared from the precursor complex [Ru(Cym)(Cl)$_2$]$_2$[11] and the ligand abpy. The asymmetrical dinuclear complex [(acac)$_2$Ru1(μ-abpy)Ru2(Cym)Cl]PF_6 ([**2**]PF_6) has been synthesized from

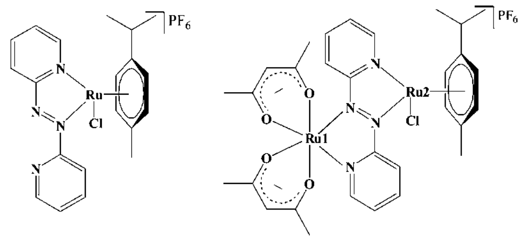

[**1**]PF_6 [**2**]PF_6

the preformed complexes [Ru(acac)$_2$(abpy)][5b] and [Ru(Cym)-(Cl)$_2$]$_2$[11] (see the Experimental Section).

The 1:1 conducting and diamagnetic [**1**]PF_6 and [**2**]PF_6 exhibit satisfactory microanalytical (C, H, and N) and mass (MS) spectral data (Figure S1 in the Supporting Information). ^{1}H NMR spectra in $CDCl_3$ show 22 (12 aromatic and 10 aliphatic) and 36 (12 aromatic and 24 aliphatic) proton signals for **1**$^+$ and **2**$^+$, respectively, within the chemical shift range of 0−10 ppm (see the Experimental Section and Figure S2 in the Supporting Information). Cation **2**$^+$ exhibits two singlets for the CH(acac) protons and four singlets for the CH_3(acac) protons, as expected for an asymmetrical complex having C_1 symmetry.

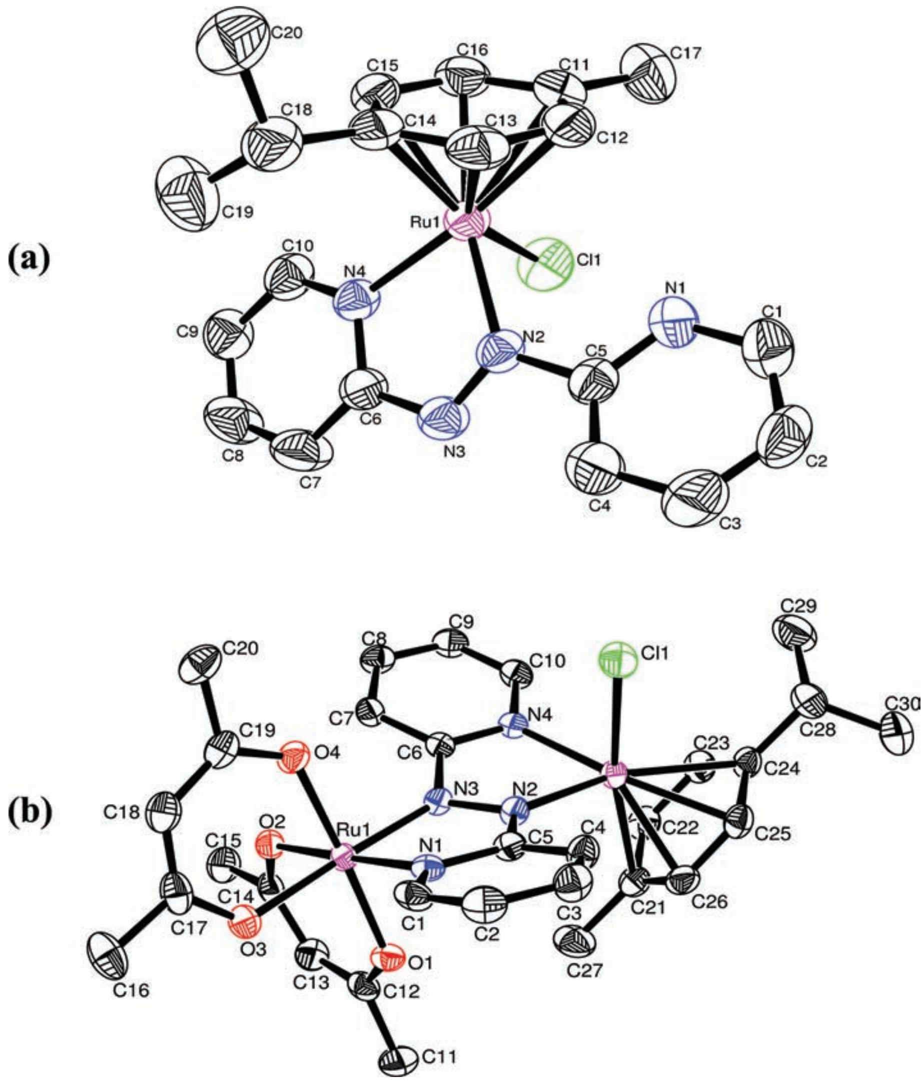

Figure 1. ORTEP diagrams of the cationic parts of (a) [**1**]PF_6 and (b) [**2**]PF_6. Ellipsoids are drawn at the 50% probability level. H atoms and the hexafluorophosphate anion are omitted for clarity.

dx.doi.org/10.1021/ic201975h | Inorg. Chem. 2012, 51, 1675−1684

Table 1. Selected Crystallographic Data for [1]PF_6 and [2]PF_6

	[1]PF_6	[2]PF_6
empirical formula	$C_{20}H_{22}ClF_6N_4PRu$	$C_{30}H_{36}ClF_6N_4O_4PRu_2$
fw	599.91	899.19
cryst syst	triclinic	orthorhombic
space group	$P\bar{1}$	*Pbca*
a (Å)	9.1440(5)	14.1822(2)
b (Å)	9.8317(5)	16.3106(3)
c (Å)	13.3061(7)	29.7326(4)
α (deg)	84.606(4)	90
β (deg)	73.940(5)	90
γ (deg)	88.789(4)	90
V (Å^3)	1144.44(10)	6877.75(18)
Z	2	8
μ (mm^{-1})	0.937	1.076
T (K)	293(2)	150(2)
D_{calcd} (g cm^{-3})	1.741	1.737
F(000)	600	3600
θ range (deg)	3.20−24.99	3.23−25.00
data/restraints/param	4012/0/301	6042/0/440
R1, wR2 [$I > 2\sigma(I)$]	0.0401, 0.0953	0.0257, 0.0604
R1, wR2 (all data)	0.0538, 0.0987	0.0389, 0.0625
GOF	0.953	0.924
largest diff peak/hole (e Å^{-3})	0.707/−0.364	0.598/−0.280

Table 2. X-ray- and DFT-Calculated Selected Bond Distances (Å) and Bond Angles (deg) for [1]PF_6

bond distance (Å)	X-ray	DFT	bond angle and torsional angle (deg)	X-ray	DFT
Ru1−N2	2.045(3)	2.063	N2−Ru1−N4	75.33(13)	75.53
Ru1−N4	2.050(3)	2.069	N2−Ru1−Cl1	85.90(9)	84.44
Ru1−C13	2.188(4)	2.269	N4−Ru1−Cl1	83.60(10)	83.82
Ru1−C15	2.204(4)	2.302	N1−C5−N2−N3	25.44	22.11
Ru1−C16	2.217(4)	2.312			
Ru1−C12	2.229(4)	2.332			
Ru1−C14	2.234(4)	2.351			
Ru1−C11	2.261(4)	2.397			
Ru1−Cl1	2.3716(12)	2.413			
N1−C5	1.314(5)	1.332			
N1−C1	1.336(6)	1.336			
N2−N3	1.269(4)	1.274			
N2−C5	1.451(5)	1.440			
N3−C6	1.395(5)	1.379			
N4−C10	1.341(5)	1.344			
N4−C6	1.354(5)	1.361			
C1−C2	1.365(7)	1.398			
C2−C3	1.352(7)	1.395			
C3−C4	1.384(6)	1.392			
C4−C5	1.360(6)	1.401			
C6−C7	1.375(6)	1.400			
C7−C8	1.371(7)	1.390			
C8−C9	1.364(6)	1.399			
C9−C10	1.374(6)	1.392			
Ru1---N1	3.286	3.356			

Mononuclear [1]PF_6. The molecular identity of [1]PF_6 has been authenticated by its single-crystal X-ray structure analysis (Figure 1a and Tables 1 and 2). The ligand abpy in [1]PF_6 is bonded to the Ru ion via the N2(azo) and N4(py) donors, forming a five-membered chelate ring. The Ru−N2(azo) and Ru−N4(py) distances of 2.045(3) and 2.050(3) Å in [1]PF_6 are significantly longer than those reported for the structurally characterized dinuclear [(μ-abpy){Ru(acac)$_2$}$_2$] (average distances: Ru−N(azo) = 1.959(3) Å for the rac isomer and 1.970(8) Å for meso isomer and Ru−N(py) = 2.007(3) Å for the rac isomer and 2.012(8) Å for the meso isomer) because of the effect of the π-accepting ancillary ligand, Cym.[5] The Ru−Cl distance of 2.3716(12) Å matches well with reported Ru^{II}−Cl distances.[12] The average Ru−C(Cym) bond distance of 2.222(4) Å is close to the values reported in other structurally characterized {Ru-Cym} complexes.[12] The N2−N3(abpy) distance, 1.269(4) Å (DFT geometry optimization: 1.274 Å) in [1]PF_6; (Table 2), indicates that the azo group is in the neutral [N═N]^0 state (Scheme 1), as reported for other mononuclear ruthenium complexes incorporating the abpy ligand.[13] The other bond distances are as expected for a mononuclear complex of the neutral abpy ligand.[13] The calculated bond parameters based on the DFT-optimized 1^+ in the singlet ground state (Figure S3a in the Supporting Information) match fairly well with the experimentally obtained data (Table 2). As for the conformation, the uncoordinated pyridine ring is twisted such that the less-space-demanding pyridyl N atom points in the direction of the metal, albeit without an actual coordination N1−Ru distance of 3.286 Å. Such an s-cis/E/s-trans conformation was observed earlier.[8] The relevant torsional angle N1−C5−N2−N3 amounts to 25.44°.

Both oxidation and reduction of [1]PF_6 are irreversible, according to cyclic voltammetry and spectroelectrochemistry in acetonitrile (Figure S4 in the Supporting Information and Table 3). DFT calculations of 1^+ show the highest occupied molecular orbital (HOMO) to HOMO−2 dominated by metal- and chloride-based orbitals (Table S1 in the Supporting Information). The presence of two π-acceptor ligands (abpy and Cym) stabilizes the Ru^{II} state, reflected by the high potential of E_{pa} = 1.67 V for the Ru^{II}/Ru^{III} transition. [1]PF_6 exhibits two irreversible reductions at −0.3 and −1.9 V versus SCE; the lowest unoccupied molecular orbital (LUMO) of 1^+ is dominated by abpy (83%; Table S1 in the Supporting Information).

In acetonitrile, 1^+ exhibits a moderately intense metal-to-ligand charge-transfer (MLCT) absorption band at 510 nm [time-dependent DFT (TD-DFT): 519 nm], in addition to intense absorption in the UV region (Figure S5 in the Supporting Information and Table 4). The feature has been assigned as a Ru(dπ)/Cl(π) → abpy(π^*) MLCT/ligand-to-ligand charge-transfer (LLCT) transition (Table S2 in the Supporting Information).

Dinuclear [2]PF_6. The molecular structure of the dinuclear cation in the crystal of complex [2]PF_6 is shown in Figure 1b. Selected crystallographic and bond parameters are listed in Tables 1 and 5, respectively. The asymmetrical dinuclear complex shows the expected "S-frame" configuration,[8] where the C−N−N−C torsional angle of the moderately twisted bis-chelating bridging abpy ligand is 22.7°. The bridging abpy is coordinated to the {Ru1(acac)$_2$} and {Ru2(Cym)Cl} components, with its N1,N3 and N2,N4 donor sets, respectively, forming five-membered chelate rings at each end. The Ru1−N3(azo) distance is about 0.1 Å shorter than the Ru1−N1(py) distance because of the strong π-back-bonding effect of Ru1 to the azo group of abpy,[5] which is being facilitated by the electron-rich acac$^-$ groups attached to the Ru1 site. Such an effect is not observed at the other terminus binding the {Ru(Cym)Cl} fragment, which exhibits comparable distances Ru2−N2(azo) [2.072(2) Å] and Ru(2)-N4(py) [2.073(2) Å]. Moreover, both Ru2−N distances are appreciably longer than the Ru1−N distances, which suggests different metal oxidation

Table 3. Electrochemical Data[a] for [1]PF_6 and [2]PF_6

complexes	$E_{298}°$ [V] (ΔE_p [mV])[b]					
	Ox$_2$	Ox$_1$	Red$_1$	Red$_2$	Red$_3$	Red$_2'$
1$^+$		1.67 (E_{pa})[c]	−0.30(90)	−1.90(100)		
2$^+$	1.62 (E_{pa})[c]	0.76(80)	−0.42(60)	−1.04 (E_{pc})[c]	−1.60(80)	−0.57 (E_{pa})[c]

[a]From cyclic voltammetry in CH_3CN/0.1 M Et_4NClO_4 at 100 mV s^{-1}. [b]Potential in V versus SCE; peak potential differences ΔE_p [mV] (in parentheses). [c]E_{pa} and E_{pc} are anodic and cathodic peak potentials, respectively.

Table 4. UV−vis−NIR Spectroelectrochemical Data for 1^n, 2^n, and 2a^n in CH_3CN/0.1M Bu_4NPF_6

complexes	λ [nm] (ε [$M^{-1}cm^{-1}$])
1$^+$	510 (4000), 360 (12 500), 300 (8600), 230 (11 800)
2^{2+}	1700 (120), 725 (13 890), 400 (15 830), 290 (18 430)
2$^+$	1600 (100), 630 (10 500), 380(10 800), 300 (18 800), 270 (23 900)
2/2a$^+$ [a]	905 (4330), 370 (17 830), 270 (26 200)
2a	1100 (sh), 860 (7270), 500 (sh), 430 (10 100), 310 (sh), 272 (31 000)
2a$^-$	870 (sh), 625 (sh), 460 (11 000), 350 (15 100), 270 (33 200)

[a]Mixture from UV−vis spectroelectrochemistry (no isosbestic point observed).

states, Ru1^{III} and Ru2^{II}. Obviously, this difference is due to the effect of the different electronic nature of the ancillary ligands, σ-donating acac$^-$ versus π-accepting Cym. Remarkably, the central azo N−N bond distance of coordinated abpy has been lengthened to 1.352(3) Å in [**2**]PF_6, which corresponds to the azo radical-anion state, $[N-N]^{\bullet-}$ (Scheme 1),[5,14] and hence to the oxidation-state assignment [(acac)$_2$Ru1^{III}(μ-abpy$^{\bullet-}$)Ru2^{II}(Cym)Cl]$^+$, i.e., *an asymmetrical mixed-valent configuration bridged by a radical ligand*. The antiferromagnetic coupling between the unpaired spins on Ru1^{III} and abpy$^{\bullet-}$ is responsible for the diamagnetic ground state of [**2**]PF_6. The change from d(NN) = 1.269(4) Å of mononuclear [**1**]PF_6 to 1.352(3) Å of dinuclear [**2**]PF_6 reveals a transfer of charge from {Ru^{II}(acac)$_2$} to the azo function under the formation of {Ru^{III}(acac)$_2$}$^+$. Similar electron transfer from {Ru^{II}(acac)$_2$} to bridging abpy has been reported earlier for the symmetrical [Ru$^{2.5}$(acac)$_2$-(μ-abpy$^{\bullet-}$)Ru$^{2.5}$(acac)$_2$] [rac, 1.372(4) Å; meso, 1.374(11) and 1.352(17) Å].[5] Other radical-anion ligand states of abpy or the related 2,2′-azobis(5-chloropyrimidine) (abcp) occur in [Os^{II}(abpy$^{\bullet-}$)(Br)(CO)(PPh$_3$)$_2$] [d(NN) = 1.348(22) Å][14a] or [Cu^I(PPh$_3$)$_2$(μ-abcp$^{\bullet-}$)Cu^I(PPh$_3$)$_2$]$^+$ [d(NN) = 1.345(7) Å].[14b]

The radical-anion nature of the abpy ligand in [**2**]PF_6 with diminished N−N bond order allows the C−N−N−C entity to be twisted by an angle of 22.7°, as has been observed earlier for *rac*- and *meso*-[Ru^{II}(acac)$_2$(μ-abpy$^{\bullet-}$)Ru^{III}(acac)$_2$].[5] The twisting leads to a rather small Ru−Ru separation of 4.745 Å. The calculated bond parameters for the DFT-optimized structure of **2**$^+$ match fairly well with the X-ray crystallographic data of [**2**]PF_6 (Figure S3b in the Supporting Information and Table 5). The calculated N−N bond distance of 1.337 Å and the C−N−N−C torsional angle of 20.87° are in agreement with the crystal data.

The dinuclear complex **2**$^+$ exhibits successive two oxidation (Ox$_1$ and Ox$_2$) and three reduction (Red$_1$, Red$_2$, and Red$_3$) processes within ±2 V versus SCE in CH_3CN (Figure 2 and Table 3). Of these, only the first oxidation is fully reversible. The first reduction leads to partial chemical reactivity,[15,16] as is evident from EPR and UV−vis spectroelectrochemistry (vide infra). The typical Ru^{III}-type[17] anisotropic EPR signal of the one-electron-oxidized species **2**$^{2+}$ (g_1 = 2.207, g_2 = 2.155, g_3 = 1.929 at 110 K; $\Delta g = g_1 - g_3$ = 0.28, $\langle g \rangle$ = 2.100; Figure 3a) can be described either with the formulation [(acac)$_2$Ru1^{III}(μ-abpy^0)Ru2^{II}(Cym)Cl]$^{2+}$ or with the combination [(acac)$_2$-Ru1^{III}(μ-abpy$^{\bullet-}$)Ru2^{III}(Cym)Cl]$^{2+}$. In the former alternative, the oxidation of abpy$^{\bullet-}$ to abpy^0 leaves the unpaired spin on the Ru^{III} ion, while in the latter, the oxidation of Ru2^{II} to Ru2^{III} leads to a three-spin situation where antiferromagnetic coupling between one of the Ru^{III} centers and abpy$^{\bullet-}$ leaves the remaining

Table 5. X-ray- and DFT-Calculated Selected Bond Distances (Å) and Bond Angles (deg) for [2]PF_6

bond distance (Å)	X-ray	DFT	bond angle (deg)	X-ray	DFT
Ru1−N3	1.916(2)	1.977	N3−Ru1−N1	78.20(9)	77.319
Ru1−N1	2.016(2)	2.057	N3−Ru1−O4	90.14(8)	92.093
Ru1−O4	2.0166(19)	2.067	N1−Ru1−O4	91.33(8)	95.004
Ru1−O1	2.0169(19)	2.0567	N3−Ru1−O1	93.38(8)	93.364
Ru1−O3	2.039(2)	2.060	N1−Ru1−O1	87.01(8)	86.346
Ru1−O2	2.0478(19)	2.087	O4−Ru1−O1	175.73(8)	174.541
Ru2−N2	2.072(2)	2.081	N3−Ru1−O3	175.26(9)	173.713
Ru2−N4	2.073(2)	2.082	N1−Ru1−O3	97.09(8)	96.437
Ru2−C22	2.156(3)	2.268	O4−Ru1−O3	90.55(8)	89.158
Ru2−C26	2.184(3)	2.280	O1−Ru1−O3	85.75(8)	85.432
Ru2−C21	2.196(3)	2.316	N3−Ru1−O2	98.39(8)	100.473
Ru2−C25	2.205(3)	2.292	N1−Ru1−O2	176.47(8)	176.973
Ru2−C23	2.214(3)	2.307	O4−Ru1−O2	89.60(8)	87.117
Ru2−C24	2.241(3)	2.351	O1−Ru1−O2	92.30(8)	91.742
Ru2−Cl1	2.3787(8)	2.414	O3−Ru1−O2	86.31(8)	85.740
N1−C1	1.340(4)	1.345	N2−Ru2−N4	75.15(9)	74.811
N1−C5	1.359(3)	1.360	N2−Ru2−Cl1	87.26(7)	87.585
N2−N3	1.352(3)	1.337	N4−Ru2−Cl1	83.42(6)	85.943
N2−C5	1.389(3)	1.383			
N3−C6	1.408(3)	1.401			
N4−C6	1.340(3)	1.356			
N4−C10	1.341(3)	1.343			
C1−C2	1.370(4)	1.388			
C2−C3	1.389(4)	1.401			
C3−C4	1.371(4)	1.387			
C4−C5	1.384(4)	1.405			
C6−C7	1.385(4)	1.399			
C7−C8	1.381(4)	1.391			
C8−C9	1.372(4)	1.396			
C9−C10	1.372(4)	1.391			

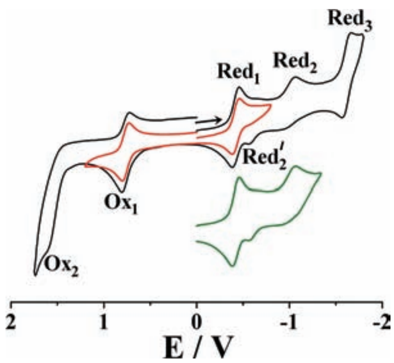

Figure 2. Cyclic voltammograms of [**2**]PF_6 (voltammograms with red and green lines correspond to segmented parts) in CH_3CN/0.1 M Et_4NClO_4 versus SCE (scan rate: 100 mV s^{-1}).

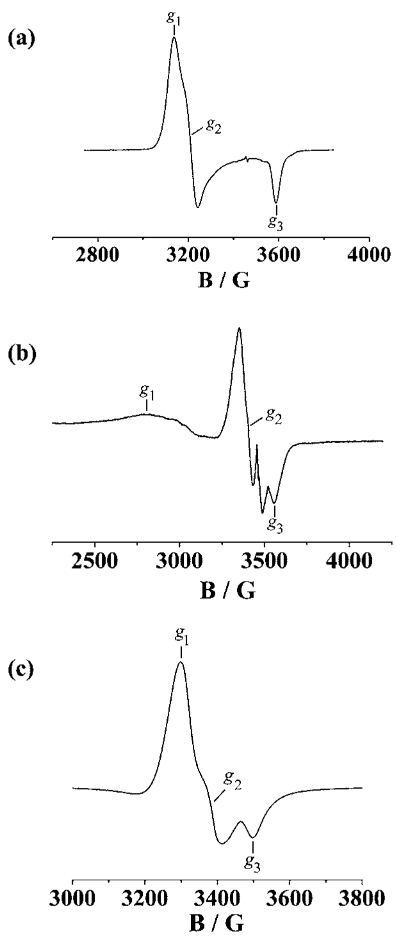

Figure 3. EPR spectra of (a) $\mathbf{2}^{2+}$ (from oxidation of [**2**]PF_6), (b) $\mathbf{2a}^{+}$/**2** (from reduction of [**2**]PF_6; g_1, g_2, and g_3 marked for $\mathbf{2a}^{+}$), and (c) $\mathbf{2a}^{-}$ (from exhaustive three-electron reduction of [**2**]PF_6) in CH_3CN/0.1 M Bu_4NPF_6 at 110 K. The additional signal at g = 2.00 in the EPR spectrum of $\mathbf{2a}^{+}$ is attributed to a decomposition species involving the abpy$^{\bullet-}$ organic radical with unknown coordination, possibly a mononuclear dissociation product.

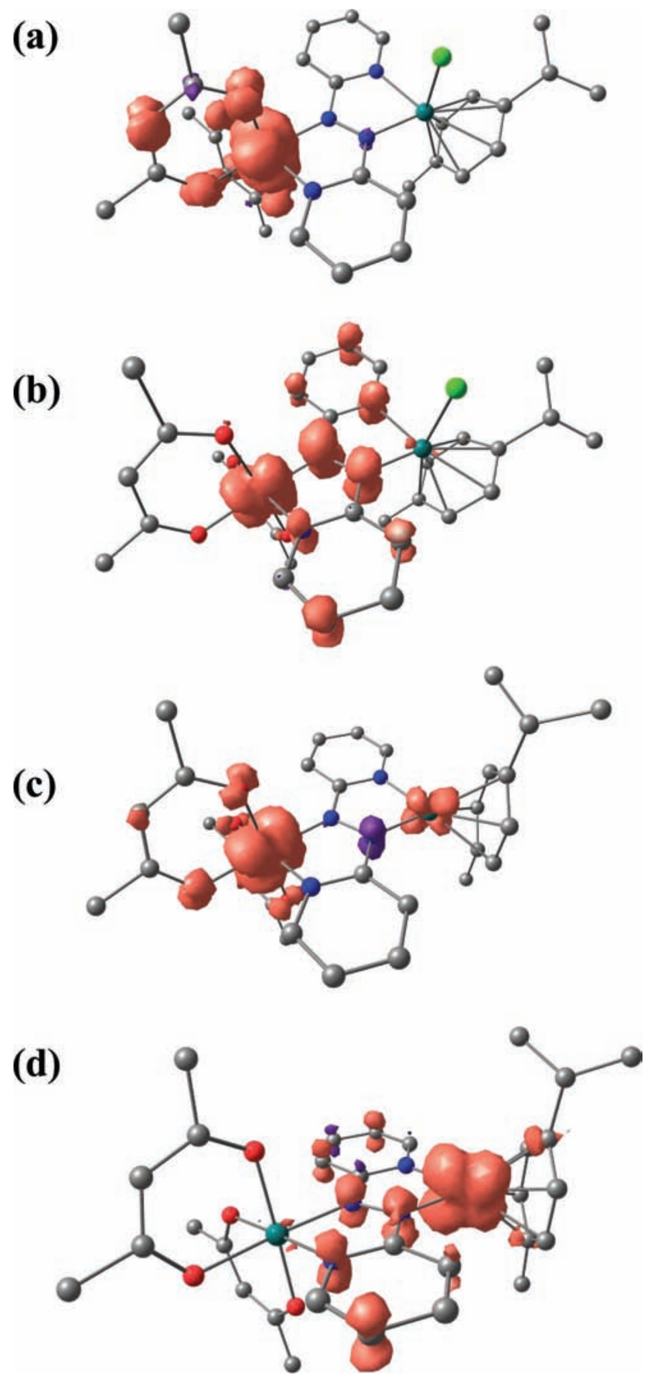

Figure 4. Spin-density representations of (a) $\mathbf{2}^{2+}$, (b) **2**, (c) $\mathbf{2a}^{+}$, and (d) $\mathbf{2a}^{-}$ in the respective doublet (S = $^1/_2$) ground state. H atoms are omitted for clarity.

spin localized at the other Ru^{III} ion. Although the composition of the HOMO of $\mathbf{2}^{+}$ (Ru1, 39%; Ru2, 4%; abpy, 20%; acac, 37%; Table S3 in the Supporting Information) seems to allow also for another formulation, viz., $[(acac)_2Ru1^{IV}(\mu\text{-abpy}^{\bullet-})Ru2^{II}(Cym)Cl]^{2+}$, the Mulliken spin densities of $\mathbf{2}^{2+}$ (Ru1, 0.727; Ru2, 0; acac, 0.334; abpy, −0.038; Figure 4a) suggest a $\{Ru1^{III}(abpy^{0})Ru2^{II}\}$ formulation, supported by the shortening of the DFT-calculated N−N bond distance from 1.337 Å in $\mathbf{2}^{+}$ (Table 5) to 1.308 Å in $\mathbf{2}^{2+}$ (Table S4 in the Supporting Information). Thus, the first oxidation process is abpy-based to yield $[(acac)_2Ru1^{III}(\mu\text{-abpy}^{0})\text{-}Ru2^{II}(Cym)Cl]^{2+}$ from $[(acac)_2Ru1^{III}(\mu\text{-abpy}^{\bullet-})Ru2^{II}(Cym)Cl]^{+}$. As a consequence, $\mathbf{2}^{2+}$ exhibits a weak $Ru2^{II} \rightarrow Ru1^{III}$ intervalence charge-transfer (IVCT) band at 1700 nm, with the metal−metal transition for the mixed-valent system being mediated through a low-lying vacant π^* orbital of abpy (see later). The low intensity of the IVCT absorption reflects poor orbital

dx.doi.org/10.1021/ic201975h | Inorg. Chem. 2012, 51, 1675−1684

Table 6. TD-DFT-Calculated (B3LYP/CPCM/CH_3CN) Electronic Transitions for 2^n (n = +, 2+)

state	energy (eV)	λ/nm (DFT)	λ/nm (exptl)	f	transition	character
					$[(acac)_2Ru^{III}(\mu\text{-abpy}^{\bullet-})Ru^{II}Cl(Cym)]^+$ (2^+) [Singlet (S = 0)]	
1	0.80	1542	1600	0.007	HOMO → LUMO (0.57), HOMO−1 → LUMO (0.25)	Ru1(dπ)/acac(π) → abpy(π*)/Ru1(dπ)
3	1.82	681	630	0.132	HOMO−1 → LUMO (0.54)	Ru1(dπ)/acac(π) → abpy(π*)
5	2.16	573	630	0.071	HOMO−4 → LUMO (0.64)	acac(π)/Ru1(dπ) → abpy(π*)
16	3.22	382	380	0.036	HOMO → LUMO+3 (0.60)	Ru1(dπ)/acac(π) → abpy(π*)
17	3.28	378	380	0.185	HOMO−9 → LUMO (0.50), HOMO−10 → LUMO (0.11)	abpy(π)/Ru2(dπ) → abpy(π*)
18	3.32	373	380	0.117	HOMO−11 → LUMO (0.34), HOMO−9 → LUMO (0.26)	acac(π)/abpy(π) → abpy(π*)
					$[(acac)_2Ru^{III}(\mu\text{-abpy})Ru^{II}Cl(Cym)]^{2+}$ (2^{2+}) [Doublet (S = $^1/_2$)]	
1	0.78	1590	1700	0.001	HOMO(β) → LUMO+1(β) (0.001)	Ru2(dπ)/Cl(pπ) → Ru1(dπ)
10	1.85	671	725	0.147	HOMO−2(α) → LUMO(α) (0.57), HOMO−1(β) → LUMO(β) (0.30)	Ru2(dπ)/Cl(pπ) → abpy(π*)
33	2.92	424	400	0.050	HOMO−7(β) → LUMO+1(β) (0.51), HOMO−7(α) → LUMO(α) (0.27)	acac(π) → Ru(dπ) abpy(π) → abpy(π*)
44	3.16	392	400	0.212	HOMO−10(α) → LUMO(α) (0.43), HOMO−7(α) → LUMO(α) (0.34)	abpy(π)/acac(π) → abpy(π*), Ru1(dπ) → abpy(π*)

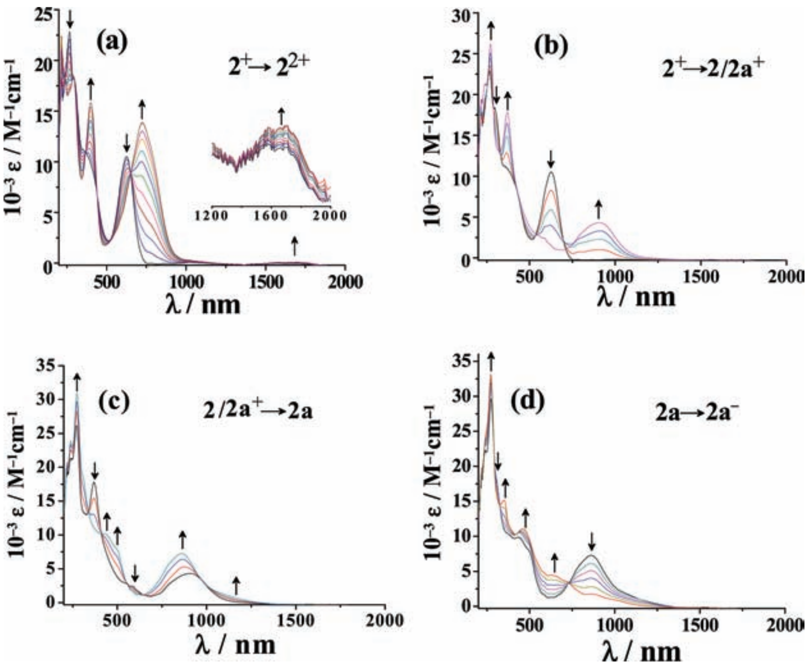

Figure 5. UV−vis−NIR spectroelectrochemistry for the conversions of (a) $2^+ \rightarrow 2^{2+}$, (b) $2^+ \rightarrow 2/2a^+$, (c) $2/2a^+ \rightarrow 2a$, and (d) $2a \rightarrow 2a^-$ in CH_3CN/0.1 M Bu_4NPF_6.

overlap in the distinctly asymmetric bis-chelate[1q] situation, although the transition energy is comparable to that of classical $Ru^{III}Ru^{II}$ mixed-valent cases such as the Creutz−Taube ion.[1a] The main intense bands of the precursor 2^+ at 630 and 380 nm are assigned to the two MLCT transitions from Ru1 and Ru2 to π*(abpy) with the help of TD-DFT calculations (Table 6). In addition to the NIR band attributed to an IVCT/metal-to-metal charge-transfer (MMCT) transition (Ru2 → Ru1), the oxidation produces intense absorptions at 725 nm (MLCT from Ru2) and 400 nm (ligand-based transitions; see Table 6).

The first one-electron reduction (Red_1, Figure 2) at −0.43 V versus SCE may lead to 2^+ from **2** with the possible formulations $[(acac)_2Ru1^{III}(\mu\text{-abpy}^{2-})Ru2^{II}(Cym)Cl]$ and $[(acac)_2Ru1^{II}(\mu\text{-abpy}^{\bullet-})\ Ru2^{II}(Cym)Cl]$ for **2**. A Ru^{III}-type EPR spectrum with widely spread g components at g_1 = 2.454, g_2 = 2.032, and g_3 = 1.947 is observed, in addition to resonances closer to g = 2 (Figure 3b). UV−vis spectroelectrochemistry, operating on a slower time scale (minutes) than standard cyclic voltammetry (Figure 2), shows changes without a proper isosbestic point (Figure 5b), which suggests the presence of more than just two species in equilibrium. Following the established reactivity pattern[7,9,15,16,18] for systems $[(L)M(C_nR_n)Cl]$, where L is a noninnocent ligand such as bpy[16] or abpy,[7,8] and M = Ru, Os with n = 6 or M = Rh, Ir with n = 5, one may consider the loss of chloride to form $[(acac)_2Ru1^{III}(\mu\text{-abpy}^{2-})Ru2^{II}(Cym)]^+$ ($2a^+$). While Mulliken spin-density calculations for **2** predict the spin equally distributed between Ru1 (0.443) and abpy (0.459) (Figure 4b), the calculation for $2a^+$ (Figure 4c) reveals much higher metal contributions for Ru1 (0.750) and Ru2 (0.134) and less participation from the ligands acac (0.162), abpy (−0.066), and Cym (0.014). The combined metal spin density of 0.884 would be in agreement with the large g anisotropy

dx.doi.org/10.1021/ic201975h | Inorg. Chem. 2012, 51, 1675−1684

observed for the major component in the EPR spectroelectrochemical reduction experiment (Figure 3b). Apparently, the presence of the electron-rich $\{(acac)_2Ru1\}$ group in abpy^{n-}-mediated π conjugation favors labilization of the chloride ligand at the remote Ru2 site even after one-electron addition (EC process), in contrast to the typical two-electron behavior.[7,9,15,16,18,19] Reduction of either **2** or chloride-depleted **2a**$^+$ yields $[(acac)_2Ru1^{II}(\mu\text{-abpy}^{2-})Ru2^{II}(Cym)]$ (**2a**) in a well-behaved manner (Figure 5c). Upon scan reversal, **2a** oxidizes to $[(acac)_2Ru1^{III}(\mu\text{-abpy}^{2-})Ru2^{II}(Cym)]^+$ at −0.57 V (Red$_2'$; Figure 2) because of slow Cl^- association at the Ru2 center. The ligand bridge abpy^{n-} can obviously act as an electron reservoir, which may facilitate dissociation of the chloride from Ru2 and thus create a coordinatively unsaturated site.

The EC process (reductive elimination) leading from **2** to **2a** is a well-documented reaction for compounds of the complex fragments $[MCl(arene)]^+$ (M = Ru, Os) and $[M(C_5R_5)]^+$ (M = Rh, Ir).[15,16,18−20] The electrochemical response (large shift of E_{pa} versus E_{pc}) and spectroelectrochemical signatures such as the emergence of an intense long-wavelength absorption are well established and observed for **2a** as well (see later). The high sensitivity toward oxidative addition and the possible dissociation of the neutral arene ligand have so far prevented crystallization for structure analysis. Corresponding mononuclear cyclopentadienyliridium compounds, however, could be structurally characterized.[18b,20c]

The quasi-reversible third reduction (Red$_3$) leads to the alternatively formulated $[(acac)_2Ru1^{II}(\mu\text{-abpy}^{2-})Ru2^{I}(Cym)]^-$/$[(acac)_2Ru1^{II}(\mu\text{-abpy}^{\bullet-})Ru2^{0}(Cym)]^-$ (**2a**$^-$). The spin-density plot of **2a**$^-$ (Figure 4d) shows that the Ru2 center is the primary spin-bearing center (0.726) with significant contribution from abpy (0.230) and similarly the calculated d(NN) distance of 1.405 Å (Table S4 in the Supporting Information) is intermediate between abpy^{2-} and abpy$^{\bullet-}$. In agreement with the metal/ligand mixed situation, the g anisotropy from EPR spectroscopy is diminished for **2a**$^-$ at $g_1 = 2.052$, $g_2 = 2.008$, and $g_3 = 1.936$ (Figure 3c); a similar situation was described for the related $[(abpy)Rh(C_5Me_5)]^-$ with $g_1 = 2.161$, $g_2 = 2.002$, and $g_3 = 1.945$.[18]

Not unexpectedly, a review of the experimental- and DFT-calculated g factors (Table S5 in the Supporting Information) reveals less satisfactory reproduction of absolute values; however, the trend **2a**$^+$ > **2**$^{2+}$ > **2a**$^-$ > **2** for the total g anisotropy $\Delta g = g_1 - g_3$ is clearly confirmed, in agreement with the amount of metal participation at the spin-density distribution (Figure 4).

In addition to the intense MLCT/LLCT band at 630 nm and more intense absorptions in the UV region (Figure 5a and Tables 4 and 6), the isolated complex [**2**]PF_6 exhibits a weak HOMO → LUMO transition in the NIR, centered at the Ru1/abpy interface. Upon one-electron oxidation to **2**$^{2+}$, the intensity of the NIR absorption increases (Figure 5a) and is calculated to have MMCT character ($Ru2^{II} \rightarrow Ru1^{III}$; Table 6). The intense MLCT band at 725 nm (TD-DFT: 671 nm) is identified as $Ru(d\pi)/Cl(\pi) \rightarrow abpy(\pi^*)$ transition.

Upon first reduction of **2**$^+$ to the doublet species $[(acac)_2Ru1^{III}(\mu\text{-abpy}^{2-})Ru2^{II}Cl(Cym)] \leftrightarrow [(acac)_2Ru1^{II}(\mu\text{-abpy}^{\bullet-})Ru2^{II}Cl(Cym)]$ (**2**) with partial Cl^- dissociation to produce **2a**$^+$, the intense low-energy MLCT band is red-shifted to 905 nm (TD-DFT: 910 nm) (Figure 5b and Tables 4 and 7) with substantial reduction in the intensity. The formation of chloride-free diamagnetic **2a** results in a shift of the MLCT band to 860 nm with intensity enhancement (Figure 5c and Tables 4 and 7). The final reduction (Red$_3$) of **2a** to $[(acac)_2Ru1^{II}(\mu\text{-abpy}^{2-})Ru2^{I}(Cym)]^- \leftrightarrow [(acac)_2Ru1^{II}(\mu\text{-abpy}^{\bullet-})Ru2^{0}(Cym)]^-$ (**2a**$^-$; Scheme 2) causes a small shift to 870 nm but a drastic decrease in the intensity (Figure 5d and Tables 4 and 7).

Summarizing, we have presented an asymmetrical mixed-valent configuration bridged by a radical-anion ligand in the form of compound $[(acac)_2Ru^{III}(\mu\text{-abpy}^{\bullet-})Ru^{II}(Cym)Cl](PF_6)$, which represents a rare example of a nondegenerate system in which the bridging ligand is redox-active. DFT calculations in connection with the experimental d(NN) distance of 1.352(3) Å confirm the oxidation-state assignment with antiferromagnetically coupled Ru^{III} and abpy radical-anion components. Reversible oxidation occurs at the bridge and produces a weakly coupled classical $Ru^{II}Ru^{III}$ mixed-valent arrangement, while stepwise reduction with concomitant chloride disssociation produces additional mixed-valent and radical species that could be analyzed spectroelectrochemically by EPR and UV−vis−NIR under support from TD-DFT calculations of spin densities and electronic transitions.

3. EXPERIMENTAL SECTION

Materials. The starting complexes $[Ru(Cym)Cl_2]_2$ (Cym = *p*-cymene),[11] $[Ru(acac)_2(abpy)]$,[5b] and the ligand 2,2′-azobis(pyridine) (abpy)[8] were prepared according to reported procedures. Other chemicals and solvents were of reagent-grade and were used without further purification. For spectroscopic and electrochemical studies, HPLC-grade solvents were used.

Physical Measurements. UV−vis−NIR studies were performed in CH_3CN/0.1 M Bu_4NPF_6 at 298 K using an optically transparent thin layer electrode cell mounted in the sample compartments of a J&M Tidas spectrophotometer.[21a] ^{1}H NMR spectra were obtained with a Bruker Avance III 400 spectrometer. The EPR measurements were made in a two-electrode capillary tube[21b] with an X-band Bruker system ESP300, equipped with a Bruker ER035 M gaussmeter and a HP 5350B microwave counter. Electrochemical measurements were performed using a PAR model 273A electrochemistry system with platinum working and auxiliary electrodes and an aqueous saturated calomel reference electrode (SCE) in a three-electrode configuration. The supporting electrolyte was Et_4NClO_4, and the solute concentration was ~10^{-3} M. The half-wave potential E_{298}° was set equal to $0.5(E_{pa} + E_{pc})$, where E_{pa} and E_{pc} are anodic and cathodic cyclic voltammetric peak potentials, respectively. Elemental analyses were carried out with a Perkin-Elmer 240C elemental analyzer. Electrospray ionization (ESI) MS spectra were recorded on a Micromass Q-ToF mass spectrometer.

Preparation of Complexes. *[RuCl(Cym)(abpy)](PF$_6$) ([**1**]PF$_6$).* A mixture containing 100 mg (0.16 mmol) of $[RuCl_2(Cym)]_2$ and 60 mg (0.32 mmol) of abpy was heated to reflux in 25 mL of ethanol under a dinitrogen atmosphere for 4 h. The initial brown solution gradually changed to deep red. After cooling, the volume was reduced to 5 mL, and 10 mL of a saturated aqueous solution of NH_4PF_6 was added. The precipitate thus obtained was filtered and washed several times with cold water and dried under vacuum. The crude solid product was then purified by column chromatography using a neutral silica gel column. The desired product was eluted with a 10:1 dichloromethane/acetonitrile mixture. Evaporation of the solvent under reduced pressure resulted in pure [**1**]PF_6. Yield: 110 mg (76%). Anal. Calcd for $C_{20}H_{22}ClF_6N_4PRu$: C, 40.00; H, 3.70; N, 9.34. Found: C, 40.12; H, 3.68; N, 9.46. ESI MS (in acetonitrile): m/z 454.81 corresponding to **1**$^+$ (calcd m/z 454.94). ^{1}H NMR in $CDCl_3$ [δ/ppm (J/Hz)]: 9.61 (d, 6.96, 1H), 8.87 (d, 7.28, 1H), 8.66 (d, 8.84, 1H), 8.27 (t, 7.76, 7.80, 1H), 8.05 (m, 2H), 7.94 (t, 7.24, 7.52, 1H), 7.74 (t, 6.36, 6.24, 1H), 6.44 (m, 2H), 6.11 (d, 7.72, 1H), 6.01 (d, 7.64, 1H), 2.6 (m, 1H), 2.27 (s, 3H), 1.00 (d, 9.68, 6H).

Table 7. TD-DFT-Calculated (B3LYP/CPCM/CH_3CN) Electronic Transitions for 2 and 2a^n (n = +, 0, −)

state	energy (eV)	λ/nm (DFT)	λ/nm (exptl)	f	transition	character
					$[(acac)_2Ru^{III}(\mu\text{-abpy}^{2-})Ru^{II}Cl(Cym)]/[(acac)_2Ru^{II}(\mu\text{-abpy}^{\bullet-})Ru^{II}Cl(Cym)]$ (**2**) [Doublet (S = 1/2)]	
3	1.36	910	905	0.097	HOMO−1(β) → LUMO(β) (0.81), HOMO−2(β) → LUMO(β) (0.25)	Ru1(dπ)/acac(π) → abpy(π*)/ Ru1(dπ)
35	3.04	408	370	0.029	HOMO(β) → LUMO+3(β) (0.55), HOMO−1(α) → LUMO+4(α) (0.23), HOMO(β) → LUMO+5(β) (0.19), HOMO(β) → LUMO+4(β) (0.18)	Ru1(dπ) → abpy(π*)/ acac(π*)
49	3.31	375	370	0.047	HOMO−2(β) → LUMO+5(β) (0.45), HOMO−8(β) → LUMO(β) (0.27)	Ru1(dπ) → acac(π*), Ru2(dπ) → Cym(π*)
52	3.34	371	370	0.076	HOMO(α) → LUMO+8(α) (0.36), HOMO−2(β) → LUMO+5(β) (0.35), HOMO−1(α) → LUMO+2(α) (0.20), HOMO(β) → LUMO+8(β) (0.14)	abpy(π) → abpy(π*), Ru1(dπ) → acac(π*)
					$[(acac)_2Ru^{III}(\mu\text{-abpy}^{2-})Ru^{II}(Cym)]$ (**2a**$^+$) [Doublet (S = 1/2)]	
5	1.57	791	*a*	0.040	HOMO−1(β) → LUMO(β) (0.58), HOMO−4(β) → LUMO+1(β) (0.38)	acac(π)/Ru1(dπ) → Ru1(dπ)/acac(π*)
10	2.21	560	*a*	0.215	HOMO(β) → LUMO+1(β) (0.57)	abpy(π)/Ru1(dπ) → Ru2(dπ)/abpy(π*)
11	2.26	548	*a*	0.082	HOMO−5(β) → LUMO(β) (0.83)	Ru2(dπ)/abpy(π) → Ru1(dπ)/acac(π*)
50	3.66	339	*a*	0.094	HOMO−8(α) → LUMO(α) (0.42), HOMO−7(β) → LUMO+1(β) (0.24)	Ru2(dπ) → abpy(π*)
					$[(acac)_2Ru^{II}(\mu\text{-abpy}^{2-})Ru^{II}(Cym)]$ (**2a**) [Singlet (S = 0)]	
1	1.28	967	1160	0.013	HOMO → LUMO (0.52), HOMO−1 → LUMO (0.44)	Ru1(dπ)/acac(π) → abpy(π*)/Ru2(dπ)
2	1.71	724	860	0.188	HOMO-1 → LUMO (0.47)	Ru1(dπ)/acac(π) → abpy(π*)/Ru2(dπ)
3	1.82	681	n.o.	0.058	HOMO−1 → LUMO (0.64)	Ru1(dπ) → abpy(π*)/ Ru2(dπ)
7	2.60	476	500	0.053	HOMO−3 → LUMO (0.49), HOMO−5 → LUMO (0.20)	Ru2(dπ) abpy(π)/acac(π) → abpy(π*)/Ru2(dπ)
11	2.82	439	430	0.038	HOMO → LUMO+2 (0.63)	Ru1(dπ) → abpy(π*)
37	3.86	321	310	0.157	HOMO−3 → LUMO+1 (0.50)	abpy(π)/acac(π) → abpy(π*)
41	3.98	311	310	0.131	HOMO−3 → LUMO+2 (0.50)	abpy(π)/acac(π) → abpy(π*)
					$[(acac)_2Ru^{II}(\mu\text{-abpy}^{2-})Ru^{I}(Cym)]$ or $[(acac)_2Ru^{II}(\mu\text{-abpy}^{\bullet-})Ru^{0}(Cym)]$ (**2a**$^-$) [Doublet (S = 1/2)]	
1	1.57	786	870	0.039	HOMO(β) → LUMO(β) (0.92)	Ru1(dπ)/abpy(π) → Ru2(dπ)/abpy(π*)
7	2.03	610	625	0.040	HOMO(α) → LUMO+3(α) (0.66), HOMO(α) → LUMO+1(α) (0.23)	abpy(π)/Ru(dπ) → acac(π*)/Cym(π*)
26	2.65	467	460	0.037	HOMO(α) → LUMO+7(α) (0.64), HOMO(α) → LUMO+8(α) (0.22)	abpy(π)/Ru(dπ) → Ru2(dπ)/ Cym(π*)
41	3.02	409	350	0.054	HOMO−3(α) → LUMO(α) (0.55), HOMO−2(β) → LUMO+1(β) (0.50)	Ru1(dπ) → acac(π*)
43	3.08	402	350	0.051	HOMO−2(α) → LUMO+2(α) (0.55), HOMO−2(α) → LUMO+3(α) (0.24), HOMO−3(α) → LUMO(α) (0.20)	Ru(dπ) → acac(π*)/ Cym(π*)

[a] Overlapping absorptions **2**/**2a**$^+$.

*[(acac)$_2$Ru(μ-abpy)RuCl(Cym)]PF$_6$ ([**2**]PF$_6$).* A total of 50 mg (0.08 mmol) of $[RuCl_2(Cym)]_2$ and 80 mg (0.16 mmol) of $[Ru(acac)_2(abpy)]$ were taken in 30 mL of ethanol, and the mixture was heated to reflux under a dinitrogen atmosphere for 6 h. The initial red color gradually changed to deep green. The solution was concentrated to 5 mL, and a saturated aqueous solution of NH_4PF_6 (10 mL) was added. The resulting dark precipitate was filtered and washed with cold water followed by drying under vacuum. The crude solid product was purified by column chromatography using a neutral silica gel column. The product was eluted by a 5:1 dichloromethane/acetonitrile mixture. Evaporation of the solvent under reduced pressure gave pure [**2**]PF$_6$. Yield: 100 mg (69%). Anal. Calcd for $C_{30}H_{36}ClF_6N_4O_4PRu_2$: C, 40.0; H, 4.03; N, 6.22. Found: C, 39.86; H, 4.16; N, 6.35. ESI MS (in acetonitrile): m/z 755.22 corresponding to **2**$^+$ (calcd m/z 755.05). ^{1}H NMR in $CDCl_3$ [δ/ppm (J/Hz)]: 9.3 (d, 6.96, 1H), 8.9 (d, 8.48, 1H), 8.2 (d, 9.2, 1H), 7.9 (m, 3H), 7.81 (t, 7.04, 7.16, 1H), 7.7 (d, 6.68, 1H), 6.07 (d, 6.2, 1H), 5.8 (m, 3H), 5.65 (s, 1H), 5.29 (s, 1H), 2.6 (m 1H), 2.45 (s, 3H), 2.16 (s, 3H), 2.12 (s, 3H), 2.03 (s, 3H), 1.97 (s, 3H) 1.18 (d, 6.92, 3H), 1.05 (d, 6.95, 3H).

Crystal Structure Determination. Single crystals of [**1**]PF$_6$ and [**2**]PF$_6$ were grown by the slow evaporation of their 3:1 and 1:1 acetonitrile/hexane solutions, respectively. The crystal data of [**1**]PF$_6$ and [**2**]PF$_6$ were collected on an Oxford X-CALIBUR-S CCD diffractometer at 293 and 150 K, respectively. All data were corrected for Lorentz polarization and absorption effects. The structures were solved and refined by full-matrix least-squares techniques on F^2 using the *SHELX-97* program.[22] H atoms were included in the refinement state using the riding model.

Computational Details. Full geometry optimizations were carried out using the DFT method at the (R)B3LYP level for **1**$^+$, **2**$^+$, **2**$^{3+}$, **2**$^-$, and **2a** and at the (U)B3LYP level for **2**$^{2+}$, **2**, **2a**$^+$, and **2a**$^-$.[23] All elements except Ru were assigned the 6-31G(d) basis set. The LANL2DZ basis set with an effective core potential was employed for the Ru atom.[24] Calculations were performed with the *Gaussian03* program package.[25] Vertical electronic excitations based on (U)-B3LYP/(R)B3LYP-optimized geometries were computed for **1**$^+$, **2**^{n} (n = +2, +, 0), and **2a**^{n} (n = +, 0, −) using the TD-DFT formalism[26] in acetonitrile using conductor-like polarizable continuum model (CPCM).[27] No symmetry constraints were imposed during structural optimizations. Calculated structures were visualized with *ChemCraft*.[28] *GaussSum*[29] was used to calculate the fractional contributions of various groups to each molecular orbital.

dx.doi.org/10.1021/ic201975h | Inorg. Chem. 2012, 51, 1675−1684

Scheme 2. Possible Oxidation and Reduction Pathways of 2^+

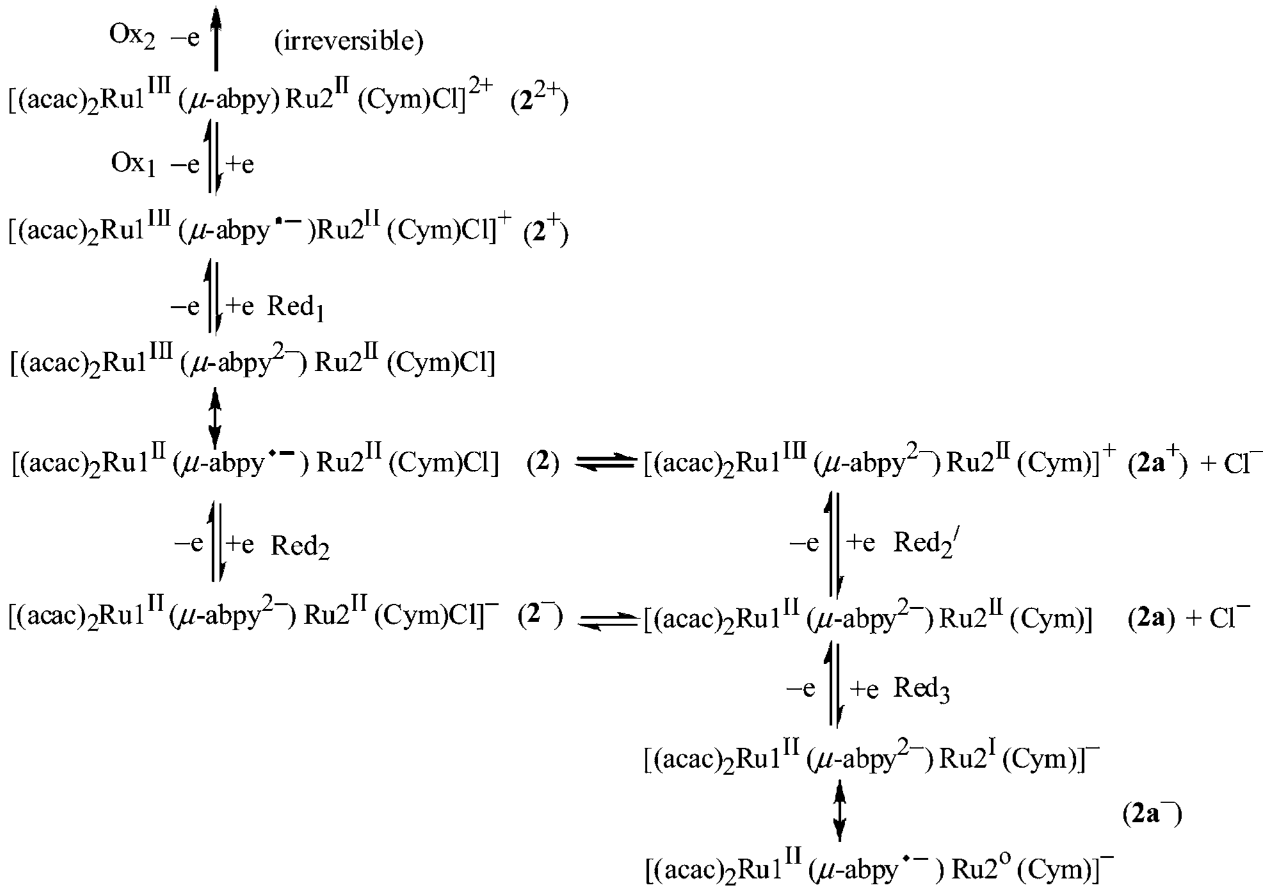

■ ASSOCIATED CONTENT

Supporting Information

X-ray crystallographic files in CIF format for $[1]PF_6$ and $[2]PF_6$, DFT data set for 1^+ and 2^+ (Tables S1−S4), experimental and calculated g factors (Table S5), MS spectra of 1^+ and 2^+ (Figure S1), ^1H NMR spectra of 1^+ and 2^+ (Figure S2), DFT-optimized structures of 1^+ and 2^+ (Figure S3), cyclic voltammograms of $[1]PF_6$ (Figure S4), UV−vis spectrum of 1^+ (Figure S5), and UV−vis−NIR spectroelectrochemistry for $2^{2+} \rightarrow 2^{3+}$ (Figure S6). This material is available free of charge via the Internet at http://pubs.acs.org.

■ AUTHOR INFORMATION

Corresponding Author

*E-mail: lahiri@chem.iitb.ac.in (G.K.L.), kaim@iac.uni-stuttgart.de (W.K.). Tel: +91 22 25767159 (G.K.L.), +49(0)711/685-64170 (W.K.). Fax: +91 22 25723480 (G.K.L.), +49(0)711/685-64165 (W.K.).

■ ACKNOWLEDGMENTS

Financial support received from the Department of Science and Technology and the Council of Scientific and Industrial Research (New Delhi, India; fellowship to A.D. and A.D.C.) and the DAAD, FCI, and DFG (Germany) is gratefully acknowledged. X-ray structural studies for $[1]PF_6$ and $[2]PF_6$ were carried out at the National Single Crystal Diffractometer Facility, Indian Institute of Technology, Bombay.

■ REFERENCES

(1) (a) Kaim, W.; Lahiri, G. K. *Angew. Chem., Int. Ed.* **2007**, *46*, 1778. (b) Masui, H.; Freda, A. L.; Zerner, M. C.; Lever, A. B. P. *Inorg. Chem.* **2000**, *39*, 141. (c) Maji, S.; Sarkar, B.; Patra, S.; Fiedler, J.; Mobin, S. M.; Puranik, V. G.; Kaim, W.; Lahiri, G. K. *Inorg. Chem.* **2006**, *45*, 1316. (d) Maji, S.; Sarkar, B.; Mobin, S. M.; Fiedler, J.; Urbanos, F. A.; Jimenez-Aparicio, R.; Kaim, W.; Lahiri, G. K. *Inorg. Chem.* **2008**, *47*, 5204. (e) Ghumaan, S.; Sarkar, B.; Maji, S.; Puranik, V. G.; Fiedler, J.; Urbanos, F. A.; Jimenez-Aparicio, R.; Kaim, W.; Lahiri, G. K. *Chem.—Eur. J.* **2008**, *14*, 10816. (f) Kumbhakar, D.; Sarkar, B.; Maji, S.; Mobin, S. M.; Fiedler, J.; Urbanos, F. A.; Jimenez-Aparicio, R.; Kaim, W.; Lahiri, G. K. *J. Am. Chem. Soc.* **2008**, *130*, 17575. (g) Das, A. K.; Sarkar, B.; Fiedler, J.; Záliš, S.; Hartenbach, I.; Strobel, S.; Lahiri, G. K.; Kaim, W. *J. Am. Chem. Soc.* **2009**, *131*, 8895. (h) Ghumaan, S.; Mukherjee, S.; Kar, S.; Roy, D.; Mobin, S. M.; Sunoj, R. B.; Lahiri, G. K. *Eur. J. Inorg. Chem.* **2006**, 4426. (i) Roy, N.; Sproules, S.; Weyhermueller, T.; Wieghardt, K. *Inorg. Chem.* **2009**, *48*, 3783. (j) Kar, S.; Sarkar, B.; Ghumaan, S.; Janardan, D.; Slageren, J. V.; Fiedler, J.; Puranik, V. G.; Sunoj, R. B.; Kaim, W.; Lahiri, G. K. *Chem.—Eur. J.* **2005**, *11*, 4901. (k) Patra, S.; Miller, T. A.; Sarkar, B.; Niemeyer, B. M.; Ward, M. D.; Lahiri, G. K. *Inorg. Chem.* **2003**, *42*, 4707. (l) Kar, S.; Sarkar, B.; Ghumaan, S.; Roy, D.; Urbanos, F. A.; Fiedler, J.; Sunoj, R. B.; Jimenez-Aparicio, R.; Kaim, W.; Lahiri, G. K. *Inorg. Chem.* **2005**, *44*, 8715. (m) Kumbhakar, D.; Sarkar, B.; Das, A.; Das, A. K.; Mobin, S. M.; Fiedler, J.; Kaim, W.; Lahiri, G. K. *Dalton Trans.* **2009**, 9645. (n) Patra, S.; Sarkar, B.; Maji, S.; Fiedler, J.; Urbanos, F. A.; Jimenez-Aparicio, R.; Kaim, W.; Lahiri, G. K. *Chem.—Eur. J.* **2006**, *12*, 489. (o) Barthram, A. M.; Cleary, R. L.; Kowallick, R.; Ward, M. D. *Chem. Commun.* **1998**, 2695. (p) Kar, S.; Sarkar, B.; Ghumaan, S.; Leboschka, M.; Fiedler, J.; Kaim, W.; Lahiri, G. K. *Dalton Trans.* **2007**, 1934. (q) Patra, S.; Sarkar, B.; Ghumaan, S.; Fiedler, J.; Kaim, W.; Lahiri, G. K. *Inorg. Chem.* **2004**, *43*, 6108.

(2) (a) Hage, R.; Haasnoot, J. G.; Nieuwenhuis, H. A.; Reedijk, J.; Ridder, D. J. A. D.; Vos, J. G. *J. Am. Chem. Soc.* **1990**, *112*, 9245. (b) Halpin, Y.; Dini, D.; Ahmed, H. M. Y.; Cassidy, L.; Browne, W. R.; Vos, J. G. *Inorg. Chem.* **2010**, *49*, 2799. (c) Ahmed, H. M. Y.; Coburn, N.; Dini, D.; Jong, J. J. D.; de Villani, C.; Browne, W. R.; Vos, J. G. *Inorg. Chem.* **2011**, *50*, 5861. (d) Heilmann, M.; Frantz, S.; Kaim, W.; Fiedler, J.; Duboc, C. *Inorg. Chim. Acta* **2006**, *359*, 821. (e) Ito, T.; Imai, N.; Yamaguchi, T.; Hamaguchi, T.; Londergan, C. H.; Kubiak, C. P. *Angew. Chem., Int. Ed.* **2004**, *43*, 1376. (f) Londergan, C. H.; Kubiak, C. P. *Chem.—Eur. J.* **2003**, *9*, 5962. (g) Salsman, J. C.; Ronco, S.; Londergan, C. H.; Kubiak, C. P. *Inorg. Chem.* **2006**, *45*, 547. (h) Salsman, J. C.; Kubiak, C. P. *J. Am. Chem. Soc.* **2005**, *127*, 2382. (i) Londergan, C. H.; Salsman, J. C.; Lear, B. J.; Kubiak, C. P. *Chem. Phys.* **2006**, *324*, 57.

(3) (a) Braun-Sand, S. B.; Wiest, O. *J. Phys. Chem. B* **2003**, *107*, 9624. (b) Braun-Sand, S. B.; Wiest, O. *J. Phys. Chem. A* **2003**, *107*, 285. (c) Wang, Y.; Lieberman, M. *IEEE Trans. Nanotechnol.* **2004**, *3*, 368. (d) Zhao, P.; Woolard, D.; Seminario, J. M.; Trew, R. *Int. J. High Speed Electron. Syst.* **2006**, *16*, 705. (e) Lent, C. S.; Isaksen, B.; Lieberman, M. *J. Am. Chem. Soc.* **2003**, *125*, 1056.

(4) LeClair, G.; Wang, Z. Y. *J. Solid State Electrochem.* **2009**, *13*, 365.

(5) (a) Sarkar, B.; Patra, S.; Fiedler, J.; Sunoj, R. B.; Janardanan, D.; Mobin, S. M.; Niemeyer, M.; Lahiri, G. K.; Kaim, W. *Angew. Chem., Int. Ed.* **2005**, *44*, 5655. (b) Sarkar, B.; Patra, S.; Fiedler, J.; Sunoj, R. B.; Janardanan, D.; Lahiri, G. K.; Kaim, W. *J. Am. Chem. Soc.* **2008**, *130*, 3532.

(6) (a) Kelso, L. S.; Reitsma, D. A.; Keene, F. R. *Inorg. Chem.* **1996**, *35*, 5144. (b) Ernst, S. D.; Kaim, W. *Inorg. Chem.* **1989**, *28*, 1520. (c) Krejcik, M.; Zalis, S.; Klima, J.; Sykora, D.; Matheis, W.; Klein, A.; Kaim, W. *Inorg. Chem.* **1993**, *32*, 3362. (d) Kohlmann, S.; Ernst, S.; Kaim, W. *Angew. Chem., Int. Ed.* **1985**, *24*, 684. (e) Ernst, S.; Kasack, V.; Kaim, W. *Inorg. Chem.* **1988**, *27*, 1146. (f) Kaim, W.; Kohlmann, S. *Inorg. Chem.* **1987**, *26*, 68.

(7) Sarkar, B.; Kaim, W.; Fiedler, J.; Duboc, C. *J. Am. Chem. Soc.* **2004**, *126*, 14706.

(8) Kaim, W. *Coord. Chem. Rev.* **2001**, *219–221*, 463.

(9) Kaim, W. In *New Trends in Molecular Electrochemistry*; Pombeiro, A. J. L., Ed.; Fontis Media: Lausanne, Switzerland, 2004; p 127.

(10) (a) Hounjet, L. J.; Ferguson, M. J.; Cowie, M. *Organometallics* **2011**, *30*, 4108. (b) Matsumura, K.; Arai, N.; Hori, K.; Saito, T.; Sayo, N.; Ohkuma, T. *J. Am. Chem. Soc.* **2011**, *133*, 10696. (c) Ito, M.; Watanabe, A.; Shibata, Y.; Ikariya, T. *Organometallics* **2010**, *29*, 4584.

(11) Bennett, M. A.; Smith, A. K. *J. Chem. Soc., Dalton Trans.* **1974**, 233.

(12) (a) Brunner, H.; Kollnberger, A.; Mehmood, A.; Tsuno, T.; Zabel, M. *Organometallics* **2004**, *23*, 4006. (b) Govindaswamy, P.; Therrien, B.; Süss-Fink, G.; Štěpnička, P.; Ludvík, J. *J. Organomet. Chem.* **2007**, *692*, 1661. (c) Pettinari, C.; Marchetti, F.; Cerquetella, A.; Pettinari, R.; Monari, M.; MacLeod, T. C. O.; Martins, L. M. D. R. S.; Pombeiro, A. J. L. *Organometallics* **2011**, *30*, 1616.

(13) (a) Oyama, D.; Asuma, A.; Hamada, T.; Takase, T. *Inorg. Chim. Acta* **2009**, *362*, 2581. (b) Fees, J.; Hausen, H. D.; Kaim, W. *Z. Naturforsch., Teil B* **1995**, *50*, 15. (c) Corral, E.; Hotze, A. C. G.; Tooke, D. M.; Spek, A. L.; Reedijk, J. *Inorg. Chim. Acta* **2006**, *359*, 830.

(14) (a) Pramanik, K.; Shivakumar, M.; Ghosh, P.; Chakravorty, A. *Inorg. Chem.* **2000**, *39*, 195. (b) Doslik, N.; Sixt, T.; Kaim, W. *Angew. Chem., Int. Ed.* **1998**, *37*, 2403.

(15) (a) Sixt, T.; Sieger, M.; Krafft, M. J.; Bubrin, D.; Fiedler, J.; Kaim, W. *Organometallics* **2010**, *29*, 5511. (b) Kaim, W.; Sixt, T.; Weber, M.; Fiedler, J. *J. Organomet. Chem.* **2001**, *637–639*, 167.

(16) Kaim, W.; Reinhardt, R.; Sieger, M. *Inorg. Chem.* **1994**, *33*, 4453.

(17) Patra, S.; Sarkar, B.; Mobin, S. M.; Kaim, W.; Lahiri, G. K. *Inorg. Chem.* **2003**, *42*, 6469.

(18) (a) Kaim, W.; Reinhardt, R.; Greulich, S.; Fiedler, J. *Organometallics* **2003**, *22*, 2240. (b) Greulich, S.; Kaim, W.; Stange, A. F.; Stoll, H.; Fiedler, J.; Záliš, S. *Inorg. Chem.* **1996**, *35*, 3998.

(19) Scheiring, T.; Fiedler, J.; Kaim, W. *Organometallics* 2001, *20*, 1437 and 3209.

(20) (a) Kölle, U.; Grätzel, M. *Angew. Chem., Int. Ed.* **1987**, *26*, 567. (b) Ladwig, M.; Kaim, W. *J. Organomet. Chem.* **1991**, *419*, 233. (c) Ziessel, R. *J. Am. Chem. Soc.* **1993**, *115*, 118.

(21) (a) Krejcik, M.; Danek, M.; Hartl, F. *J. Electroanal. Chem.* **1991**, *317*, 179. (b) Kaim, W.; Ernst, S.; Kasack, V. *J. Am. Chem. Soc.* **1990**, *112*, 173.

(22) Sheldrick, G. M. *SHELX-97, Program for Crystal Structure Solution and Refinement*; University of Göttingen: Göttingen, Germany, 1997.

(23) Lee, C.; Yang, W.; Parr, R. G. *Phys. Rev. B* **1988**, *37*, 785.

(24) (a) Dunning, T. H. Jr.; Hay, P. J. In *Modern Theoretical Chemistry*; Schaefer, H. F., III, Ed.; Plenum: New York, 1976; p 1. (b) Hay, P. J.; Wadt, W. R. *J. Chem. Phys.* **1985**, *82*, 299.

(25) Frisch, M. J.; Trucks, G. W.; Schlegel, H. B.; Scuseria, G. E.; Robb, M. A.; Cheeseman, J. R.; Montgomery, J. A., Jr.; Vreven, T.; Kudin, K. N.; Burant, J. C.; Millam, J. M.; Iyengar, S. S.; Tomasi, J.; Barone, V.; Mennucci, B.; Cossi, M. ; Scalmani, G.; Rega, N.; Petersson, G. A.; Nakatsuji, H.; Hada, M.; Ehara, M.; Toyota, K.; Fukuda, R.; Hasegawa, J.; Ishida, M.; Nakajima, T.; Honda, Y.; Kitao, O.; Nakai, H.; Klene, M.; Li, X.; Knox, J. E.; Hratchian, H. P.; Cross, J. B.; Bakken, V.; Adamo, C.; Jaramillo, J.; Gomperts, R.; Stratmann, R. E.; Yazyev, O.; Austin, A. J.; Cammi, R.; Pomelli, C.; Ochterski, J. W.; Ayala, P. Y.; Morokuma, K.; Voth, G. A.; Salvador, P. ; Dannenberg, J. J.; Zakrzewski, V. G. ; Dapprich, S.; Daniels, A. D.; Strain, M. C.; Farkas, O.; Malick, D. K.; Rabuck, A. D.; Raghavachari, K.; Foresman, J. B.; Ortiz, J. V.; Cui, Q.; Baboul, A. G.; Clifford, S.; Cioslowski, J.; Stefanov, B. B.; Liu, G.; Liashenko, A.; Piskorz, P.; Komaromi, I.; Martin, R. L.; Fox, D. J.; Keith, T.; Al-Laham, M. A.; Peng, C. Y.; Nanayakkara, A.; Challacombe, M.; Gill, P. M. W.; Johnson, B.; Chen, W.; Wong, M. W.; Gonzalez, C.; Pople, J. A. *Gaussian 03*, revision C.02; Gaussian, Inc.: Wallingford, CT, 2004.

(26) (a) Bauernschmitt, R.; Ahlrichs, R. *Chem. Phys. Lett.* **1996**, *256*, 454. (b) Stratmann, R. E.; Scuseria, G. E.; Frisch, M. J. *J. Chem. Phys.* **1998**, *109*, 8218. (c) Casida, M. E.; Jamorski, C.; Casida, K. C.; Salahub, D. R. *J. Chem. Phys.* **1998**, *108*, 4439.

(27) (a) Barone, V.; Cossi, M. *J. Phys. Chem. A* **1998**, *102*, 1995. (b) Cossi, M.; Barone, V. *J. Chem. Phys.* **2001**, *115*, 4708. (c) Cossi, M.; Rega, N.; Scalmani, G.; Barone, V. *J. Comput. Chem.* **2003**, *24*, 669.

(28) Zhurko, D. A. Zhurko, G. A. *ChemCraft 1.5*; Plimus: San Diego, CA. http://www.chemcraftprog.com (accessed Sept 2011).

(29) (a) O'Boyle, N. M. *GaussSum 2.1*, 2007. Available at http://gausssum.sf.net (accessed Sept 2011). (b) O'Boyle, N. M.; Tenderholt, A. L.; Langner, K. M. *J. Comput. Chem.* **2008**, *29*, 839.